*Published online 28 February 2012* *Nucleic Acids Research, 2012, Vol. 40, No. 12* ***5739–5750***
*doi:10.1093/nar/gks194*

# Structural and functional characterization of interactions involving the Tfb1 subunit of TFIIH and the NER factor Rad2

**Julien Lafrance-Vanasse[1], Geneviève Arseneault[1], Laurent Cappadocia[1], Hung-Ta Chen[2], Pascale Legault[1] and James G. Omichinski[1,*]**

[1]Département de Biochimie, Université de Montréal, C.P. 6128, Succursale Centre-Ville, Montréal, QC H3C 3J7, Canada and [2]Institute of Molecular Biology, Academia Sinica, Taipei 115, Taiwan, Republic of China

Received December 20, 2011; Revised February 4, 2012; Accepted February 9, 2012

## ABSTRACT

**The general transcription factor IIH (TFIIH) plays crucial roles in transcription as part of the pre-initiation complex (PIC) and in DNA repair as part of the nucleotide excision repair (NER) machinery. During NER, TFIIH recruits the 3′-endonuclease Rad2 to damaged DNA. In this manuscript, we functionally and structurally characterized the interaction between the Tfb1 subunit of TFIIH and Rad2. We show that deletion of either the PH domain of Tfb1 (Tfb1PH) or several segments of the Rad2 spacer region yield yeast with enhanced sensitivity to UV irradiation. Isothermal titration calorimetry studies demonstrate that two acidic segments of the Rad2 spacer bind to Tfb1PH with nanomolar affinity. Structure determination of a Rad2–Tfb1PH complex indicates that Rad2 binds to TFIIH using a similar motif as TFIIEα uses to bind TFIIH in the PIC. Together, these results provide a mechanistic bridge between the role of TFIIH in transcription and DNA repair.**

## INTRODUCTION

The general transcription factor IIH (TFIIH) plays crucial roles in both transcription as part of the pre-initiation complex (PIC) and in DNA repair as part of the nucleotide excision repair (NER) machinery (1). The human TFIIH complex and the highly homologous budding yeast (*Saccharomyces cerevisiae*) counterpart are composed of 10 subunits that can be divided in two sub-complexes, the core TFIIH complex [XPB/Ssl2, XPD/Rad3, p62/Tfb1, p52/Tfb2, p44/Ssl1, p34/Tfb4 and TTDA/Tfb5 (human/yeast)] and the CAK complex (cdk7/Kin28, cyclin H/Ccl1 and MAT1/Tfb3). As a component of the PIC, TFIIH is the only general transcription factor (GTF) to possess enzymatic activity. TFIIH helicase activities (XPB/Ssl2 and XPD/Rad3) are essential to the formation of the open complex during initiation (2), whereas its kinase activity (cdk7/Kin28) is required for the phosphorylation of the carboxyl-terminal domain (CTD) of RNA polymerase II (RNAP II) (3). As part of the NER machinery, TFIIH helps recruit other repair factors to the damaged DNA (4) and through its helicase activity assists in the elimination of helix-distorted DNA typically caused by UV-induced modifications of bases (5).

NER can be divided into two distinct pathways that differ in their mechanism of initial recognition of the damaged DNA (6). In transcription-coupled NER (TC-NER), RNAP II stalls on the damaged DNA site and recruits the Cockayne Syndrome group B protein (CSB/Rad26), whereas in global genome NER (GG-NER), the damaged site is recognized by the XPC–RAD23B/Rad4–Rad23 complex in combination with UV-damaged DNA-binding proteins (UV-DDBs). Following recognition of the damaged DNA site, the two NER pathways employ a series of common steps that include recruitment of TFIIH to the lesion to unwind the DNA, displacement of either the XPC–RAD23B or RNAPII–CSB complex by the 3′-endonuclease XPG/Rad2, recruitment of XPA/Rad14 and recruitment of the 5′ endonuclease complex ERCC1–XPF/Rad10–Rad1. In both NER pathways, TFIIH functions by recruiting and stabilizing XPG/Rad2 on the damaged site (7).

XPG/Rad2 is a member of the flap-endonuclease (FEN) family of single-stranded DNA endonucleases that includes FEN-1, EXO-1 (exonuclease-1) and GEN-1 (gap endonuclease-1) (8). Based on sequence alignment,

*To whom correspondence should be addressed. Tel: +1 514 343 7341; Fax: +1 514 343 2210; Email: jg.omichinski@umontreal.ca

The authors wish it to be known that, in their opinion, the first two authors should be regarded as joint First Authors.

the N (N-terminal) and I (internal) regions are highly conserved in all family members, and a variable-length spacer region (usually 20–70 residues) separates these two conserved regions. The crystal structure of a FEN-1–DNA complex demonstrated that the N and I region come together to form a single structural domain that serves as the catalytic core of the enzyme (9). XPG/Rad2 is an atypical member of the FEN family due to the fact that it contains an extended-spacer of over 600 amino acids. This extended spacer of XPG/Rad2 is highly acidic and is mostly disordered based on secondary structure predictions (10). This intrinsically disordered nature of the spacer region of Rad2 enables it to participate in protein–protein interactions with several different proteins including multiple subunits of TFIIH (10–13).

The interaction between TFIIH and XPG/Rad2 is essential in NER for both the recruitment of XPG/Rad2 to the repair complex and for the stabilization of the repair complex on the damaged DNA (14). Mutations in both XPG and several TFIIH subunits are associated with DNA-repair associated diseases such as Xeroderma Pigmentosum (XP) and Cockayne Syndrome (CS) (15). Formation of the TFIIH–XPG/Rad2 complex involves multiple regions of XPG/Rad2 and several subunits of TFIIH including p62/Tfb1, XPB/Ssl2, XPD/Rad3 and p44/Ssl1 (12,16). In the case of XPG, residues between 184–210, 225–231, 554–730 in the spacer region and residues 1012–1186 in the C terminus have all been shown to play a role stabilizing the interaction with TFIIH and for optimal repair of DNA damage (10,11). Based on these results, it was postulated that different subunits of TFIIH form a series of interactions with XPG/Rad2 (10).

Several studies have shown that the p62/Tfb1 subunit of TFIIH plays a role in DNA-damage repair. Deletion of the extreme carboxyl-terminal (C-terminal) region (residues 532–642) of Tfb1 leads to a yeast mutant (*tfb1-1*) with decreased resistance to both temperature and UV irradiation (17). Other studies showed that Tfb1 directly interacts with Rad2, and that this interaction requires an acid-rich segment within the extended spacer region (13). In addition, the pleckstrin homology (PH) domain of human p62 (residues 1–108) directly binds to XPG, and deletion of this domain decreases the activity of XPG in an *in vitro* repair assay (18). The PH domains of p62 and Tfb1 (p62PH/Tfb1PH) are highly homologous and have been shown to bind acidic-rich domains present in several transcriptional regulatory proteins, including the large subunit of the general transcription factor IIE (TFIIEα) (19), the tumor suppressor protein p53 (20) and the Herpes Simplex Virion protein 16 (VP16) (21).

In this article, we evaluate the functional and structural roles of the PH domain of Tfb1 (Tfb1PH) in UV-damage repair. We demonstrate that deletion of Tfb1PH (residues 1–115) yields a yeast phenotype with a decreased resistance to UV irradiation. We then identify two acidic stretches within the spacer region of Rad2 ($Rad2_{359–383}$ and $Rad2_{642–690}$) that bind to Tfb1PH with nanomolar affinity. In addition, deletion of these two acidic segments in combination with a deletion corresponding to residues 225–231 of XPG ($Rad2_{228–237}$) enhances the photosensitivity of yeast (11). We also determine the NMR structure of a complex between Tfb1PH and $Rad2_{642–690}$ and show that Rad2 binds to Tfb1PH in a very similar manner as TFIIEα binds to the p62PH (22). These results indicate that the recruitment of Rad2 to the TFIIH complex requires multiple interactions within the spacer region, and that Rad2 binds to TFIIH by a similar mechanism as TFIIEα binds TFIIH in the PIC.

## MATERIALS AND METHODS

### Strains, media and vectors

All *S. cerevisiae* strains used are listed in Supplementary Table S1. The *rad52* strain was a gift from Dr Pascal Chartrand (Université de Montréal) and the SHY186 strain was a gift from Dr Steve Hahn (Fred Hutchinson Cancer Research Center). All strains were grown either in a synthetic complete media (SC; 0.67% yeast nitrogen base without amino acids, 2% glucose and a mixture of amino acids and vitamins) lacking either tryptophan and leucine (SC-LW) or uracil (SC-U) to be selective or in a rich media (YPD; 1% yeast extract, 2% tryptone and 2% glucose). All yeast transformations were done using the modified lithium acetate protocol (23).

### Plasmid preparation

The pRS314TFB1-6His plasmid (*TFB1*) was kindly provided by the laboratory of Dr S. Hahn. From this plasmid were constructed the N-terminal and C-terminal mutants, pRS314TFB1(Δ1-115)-6His (*tfb1-ΔPH*) and pRS314TFB1(Δ532-642)-6His (*tfb1-1*), respectively. The pRS316RAD2cmyc plasmid (*RAD2*) was generated by amplification of the *RAD2* open reading frame (ORF) complemented by 400-bp upstream and 366-bp downstream on genomic DNA and insertion into pRS316. Mutant plasmids were obtained by overlapped PCR or QuikChange site-directed mutagenesis procedure (Stratagene). For details of the plasmid preparation, see Supplementary Methods.

### Plasmid shuffling

Since *TFB1* is an essential gene, plasmid shuffling was done in SHY186 to express the mutants in the *tfb1* (*TFB1* knockout) background. pRS314TFB1WT-6His, pRS314TFB1(Δ1-115)-6His and pRS314TFB1(Δ532-642)-6His were individually transformed into SHY186 and selected on SC-LWU plates to obtain the wild-type *TFB1*, *tfb1-ΔPH* mutant and *tfb1-1* mutant strains, respectively. The strains bearing the two plasmids were then grown 4 days in liquid SC-LW to remove the uracil pYCP50/TFB1-6His plasmid. During this period, the cultures were diluted (1/50) each day with fresh media. In the final dilution, 5-Fluoroorotic Acid (5-FOA; 1 mg/ml, Zymo Research) was added. The cells were then plated on SC-LW media and auxotrophy for uracil and/or tryptophan was analyzed on selective plates.

### Sensitivity assays

Yeast strains were grown overnight at 30°C in complete, selective or YPD media, as indicated. The next day they were diluted to obtain an $OD_{595} = 0.5–1$. The cells were then harvested by centrifugation, washed and resuspended in sterile water to obtain an $OD_{595} = 0.5$. For UV-sensitivity assays, dilutions were plated on selective media (SC-LW for Tfb1 and SC-U for Rad2) and irradiated with UV light (XL-1000 UV crosslinker, SpectroLinker) at varying energy levels. The surviving colonies were counted after 3 days in the dark at 30°C. For bleomycin and temperature sensitivity assays, serial 10-fold dilutions ($10^{-1}$–$10^{-4}$) were made and 8 µl of each dilution was dropped on solid media: YPD ± 250 ng/ml bleomycin and SC-LW, respectively. For the temperature sensitivity assays, the plates were incubated for 3 days at 30°C and 37°C. For the bleomycin assay, the plates were incubated for 4 days at room temperature.

### Cloning and purification of proteins

The GST–Tfb1PH (residues 1–115 of Tfb1) and GST–p53TAD2 (residues 20–73 of p53) were prepared as described (24). GST–$Rad2_{359–383}$, GST–$Rad2_{642–760}$ and GST–$Rad2_{692–760}$ were prepared by inserting the appropriate region of Rad2 (Open Biosystems) into the pGEX-2T expression vector. The GST–$Rad2_{642–690}$ was created from GST–$Rad2_{642–760}$ by inserting a stop codon and adding a tyrosine at the C terminus (for spectrophotometry $A_{280}$ quantification). All point mutants were made using the QuikChange II site-directed mutagenesis procedure (Stratagene). All coding sequences were verified by DNA sequencing. Tfb1PH and p53TAD2 were purified as described (24). Rad2 fragments and mutants were expressed as GST-fusion proteins in *E. coli* host strain TOPP2 purified over GSH resin (GE Healthcare) and cleaved with thrombin (Calbiochem) as previously described for Tfb1PH (24). Following cleavage with thrombin, the Rad2 proteins were purified over a Q-Sepharose High Performance (GE Healthcare) column and dialyzed into appropriate buffers for isothermal titration calorimetry (ITC) and nuclear magnetic resonance (NMR) studies. $^{15}N$-labeled and $^{15}N/^{13}C$-labeled proteins were prepared in M9-minimal media containing $^{15}NH_4Cl$ (Sigma) and/or $^{13}C_6$-glucose (Sigma) as the sole nitrogen and carbon sources, respectively. For all experiments, the concentrations of proteins were determined from $A_{280}$.

### ITC experiments

ITC titrations were performed as described (25), at 25°C in 20 mM sodium phosphate buffer (pH 7.5). All titrations fit a single-binding site mechanism with 1:1 stoichiometry and values are the average of two or more separate experiments.

### NMR experiments

The NMR chemical shift perturbation and competition experiments were performed as previously described (for sample details please see Supplementary Methods). For the NMR structural studies of the $Rad2_{642–690}$–Tfb1PH complex, four different samples containing 1.0 mM of the complex in a 1:1.25 ratio were used ($^{15}N$–Tfb1PH–$Rad2_{642–690}$, $^{15}N/^{13}C$–Tfb1PH–$Rad2_{642–690}$, $^{15}N$–$Rad2_{642–690}$–Tfb1PH and $^{15}N/^{13}C$–$Rad2_{642–690}$–Tfb1PH, respectively). All NMR experiments were carried out in 20 mM sodium phosphate (pH 6.5), 1 mM EDTA, 1 mM DTT and 90%$H_2O$/10% $D_2O$ or 100% $D_2O$, at 300 K on Varian Unity Inova 500, 600 and 800 MHz spectrometers equipped with z pulsed-field gradient units and triple resonance probes. All of the $^1H$, $^{15}N$ and $^{13}C$ resonances for $Rad2_{642–690}$ and Tfb1PH were assigned as reported for free Tfb1PH (26). Briefly, 3D HNCO (27), 3D HNCACB (28), 3D CBCACONH (29), 3D (H)C(CO)NH (30), 3D H(CCO)NH (30) and 3D HCCH–COSY (31) were used to assign the backbone and aliphatic side chains resonances. The aromatic side chains $^1H$, $^{13}C$ and $^{15}N$ resonances were assigned using a combination of 2D (HB)CB(CGCD)HD and 2D (HB)CB(CGCDCE)HE spectra (32). Interproton distance restraints were measured from 3D $^{15}N$-edited NOESY-HSQC and $^{13}C$-edited HMQC-NOESY spectra ($\tau_m = 90$ ms) and intermolecular distance restraints from 3D $^{15}N/^{13}C$ {F1}-filtered, {F3}-edited NOESY experiment ($\tau_m = 90$ ms) (33,34). The NMR data were processed with NMRPipe/NMRDraw (35) and analyzed with NMRView (36) and Analysis from the CCPNMR suite (37).

### Structure calculations

The NOE-derived distance restraints were divided into four classes defined as strong (1.8–2.8 Å), medium (1.8–4.0 Å), weak (1.8–5.0 Å) and very weak (3.3–6.0 Å). Backbone dihedral angles were derived with the program TALOS+ (38). The structure of the $Rad2_{642–690}$–Tfb1PH complex was calculated using the program CNS (39). The quality of the structures was analyzed by the programs PROCHECK-NMR (40) and MOLMOL (41). The figures were generated with the program PyMol (42).

## RESULTS

### *tfb1-ΔPH* yeast display enhanced sensitivity to UV damage

To investigate the *in vivo* role of the PH domain of the Tfb1 (Tfb1PH) in repair of damaged DNA, we constructed a *tfb1-ΔPH* mutant strain (deletion of residues 1–115). First, we tested the sensitivity of the *tfb1-ΔPH* yeast to UV irradiation and compared it to the wild-type *TFB1* and the *tfb1-1* yeast strains. The *tfb1-1* mutant yeast strain serves as our positive control as it has been shown to have decreased resistance to UV irradiation (17). The survival curves show that both *tfb1-ΔPH* and *tfb1-1* are significantly more sensitive to UV irradiation than the *TFB1* wild-type strain (Figure 1a). The photosensitivity of the *tfb1-ΔPH* yeast to UV irradiation is not due to a decrease in protein levels as the Tfb1-ΔPH and Tfb1 proteins are expressed at similar levels (Supplementary Figure S1a). Next, we performed drop tests to evaluate the ability of *tfb1-ΔPH* to repair DNA damage induced by bleomycin. The *tfb1* wild-type strain, the *tfb1-ΔPH* mutant strain and a *rad2* strain (*RAD2* knockout)

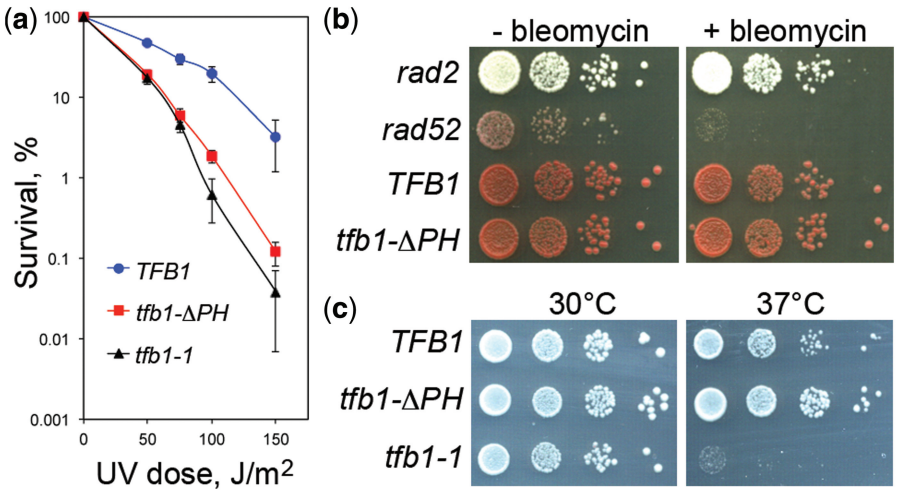


**Figure 1.** *tfb1-ΔPH* is sensitive to UV irradiation, but not bleomycin or temperature. (**a**) The survival of *TFB1* (blue), *tfb1-ΔPH* (red) and *tfb1-1* (+ control; black) yeast was determined following increasing doses of UV irradiation. The *y*-axis represents the percentage of surviving cells (normalized to the number of viable cells not exposed to UV light) and the *x*-axis shows the energy level of the UV irradiation applied ($J/m^2$). The results are the mean ± SEM of three independent experiments. (**b**) The survival of *TFB1*, *tfb1-ΔPH*, *rad2* (− control) and *rad52* (+ control) yeast was determined before (left) or after (right) exposure to bleomycin. The yeast strains were incubated on plates containing YPD ± 250 ng/ml bleomycin and survivors were determined by spotting 8 µl of cells in serial dilutions ($10^{-1}$–$10^{-4}$). The assay was repeated three times, and a typical set of results is shown. (**c**) The survival of *TFB1* (− control), *tfb1-ΔPH* and *tfb1-1* (+ control) yeast was determined following growth at either 30°C (left) or 37°C (right). The survivors were assayed by spotting 8 µl of cells in serial dilutions ($10^{-1}$–$10^{-4}$) on SC-LW plates. This assay was repeated three times and a typical set of results is shown.

all grow similarly in either the presence or absence of bleomycin and the only strain displaying enhanced sensitivity to bleomycin is the *rad52* (*RAD52* knockout) positive control (Figure 1b). Taken together, these results suggest that Tfb1PH plays a specific role in NER induced by UV irradiation.

### *tfb1-ΔPH* yeast show normal growth at 37°C

In addition to displaying a UV sensitivity phenotype, the *tfb1-1* yeast are also sensitive to growth at high temperatures (17). Therefore, we tested whether or not *tfb1-ΔPH* yeast also display a similar growth phenotype. The *TFB1*, *tfb1-ΔPH* and *tfb1-1* yeast were all grown at both 30°C and 37°C, and the drop test shows that *tfb1-1* is the only strain sensitive to growth at 37°C (Figure 1c). The *tfb1-ΔPH* and the *TFB1* strains grow similarly when incubated at 37°C, indicating that the PH domain of the Tfb1 protein is not required for growth at higher temperatures. This further supports that the sensitivity to UV irradiation observed with the *tfb1-ΔPH* strain is due to a loss of function associated with removal of Tfb1PH and not to instability associated with the protein as seen with the truncated protein expressed by *tfb1-1* yeast at 37°C.

### An acid-rich segment of the Rad2 spacer region binds Tfb1PH with high affinity

Previous studies have shown that Rad2 interacts with Tfb1 and residues 642–900 of Rad2 are sufficient for binding (13). This Tfb1-binding region of Rad2 includes an acid-rich segment from the spacer region (residues 642–760) that is required for the interaction (13). Based on these results and the fact that p62PH was shown to be required for interaction with XPG (18), we were interested to determine if the acid-rich segment between residues 642–760 of Rad2 binds directly to Tfb1PH. To test this, the apparent dissociation constant ($K_d$) for the interaction between Tfb1PH and $Rad2_{642–760}$ was determined by ITC experiments. The ITC experiments show that there is an interaction between these two protein segments, but the stoichiometry of the binding ($N = 0.52$) suggests that $Rad2_{642–760}$ contains two distinct Tfb1PH-binding sites (Supplementary Figure S2a).

Based on sequence comparison with known Tfb1PH/p62PH-binding sites from the C-terminal domain of TFIIEα (TFIIEαCTD) (22) and the transactivation domains (TADs) of p53 (p53TAD2) (20) and VP16 (VP16C) (21), we identify three segments within $Rad2_{642–760}$ (residues 661–681, 708–728 and 718–738) that could potentially contain a Tfb1PH-binding site (Figure 2). Preliminary NMR studies show that $Rad2_{642–760}$ is disordered in the unbound form as predicted (Supplementary Figure S2b). Given the fact that $Rad2_{642–760}$ is disordered and that two of the three sites overlap (650–670 and 661–681), we chose to partition $Rad2_{642–760}$ into two segments ($Rad2_{642–690}$ and $Rad2_{692–760}$) to determine the $K_d$ values of the individual segments (Figure 2b). By ITC, we determine that $Rad2_{642–690}$ ($K_d$ = 190 nM) binds with much higher affinity to Tfb1PH than $Rad2_{692–760}$ ($K_d$ = 4.6 µM). These results support the presence of two binding sites and indicate that Tfb1PH binds preferentially to the segment $Rad2_{642–690}$.

The Tfb1PH/p62PH binding sites from TFIIEαCTD, p53TAD2 and VP16C all contain hydrophobic residues that are crucial for forming the interaction interface (19–21). Based on sequence alignment, we postulate that

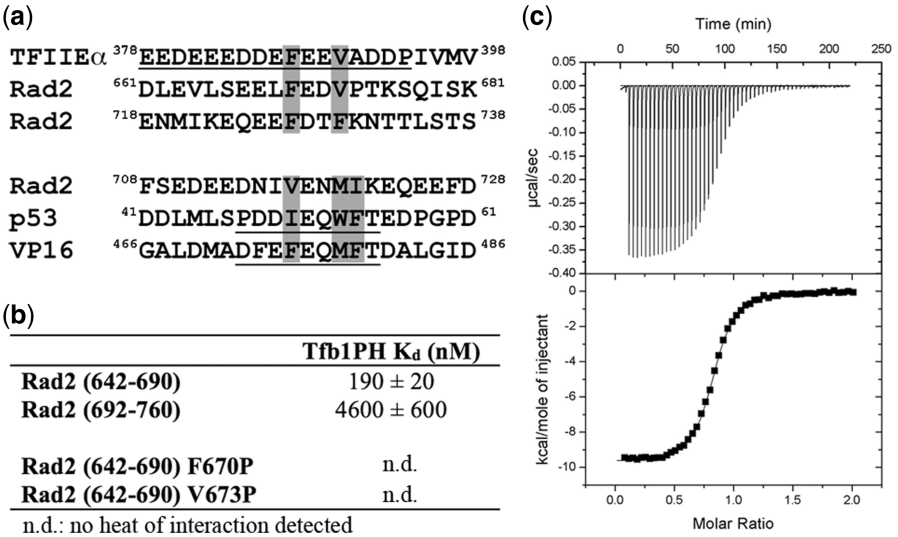


**Figure 2.** The Rad2 spacer region contains a high affinity Tfb1PH-binding site between residues 642 and 690. (**a**) Identification of amino acid segments located between residues 642–760 from the Rad2 spacer region that align with the Tfb1PH-binding sites from TFIIEαCTD, p53TAD2 and VP16C. In the alignments, the residues of TFIIEαCTD, p53TAD2 and VP16C that form the binding site with p62PH/Tfb1PH are underlined and crucial hydrophobic residues are shaded in gray. (**b**) Comparison of the dissociation constant ($K_d$) values for the binding of different Rad2 segments located between residues 642 and 760 with Tfb1PH. (**c**) Thermogram of the Tfb1PH titration with successive additions of $Rad2_{642–690}$. Experiments are performed at 25°C, in 20 mM $NaPO_4$ pH 7.5, and the results fit to a single-binding site model with 1:1 stoichiometry.

Phe670 and Val673 of $Rad2_{642–690}$ play an important role in forming the interface between $Rad2_{642–690}$ and Tfb1PH. To test the importance of these two hydrophobic residues, we prepared proline mutants (F670P and V673P) and measured their binding to Tfb1PH by ITC. The ITC studies show that neither the F670P nor V673P mutant of $Rad2_{642–690}$ bind with appreciable affinity.

### $Rad2_{642–690}$, p53TAD2 and TFIIEαCTD bind a common site on Tfb1PH

To identify the binding site for $Rad2_{642–690}$ on Tfb1PH, NMR chemical shift perturbation studies were performed. In these experiments, addition of unlabeled $Rad2_{642–690}$ to $^{15}$N-labeled Tfb1PH cause significant changes in the $^{1}$H and $^{15}$N chemical shifts for several Tfb1PH signals in the $^{1}$H–$^{15}$N HSQC spectrum (Supplementary Figure S3a and S3b). When mapped onto the structure of Tfb1PH, the residues exhibiting significant chemical shift changes are located in strands β5, β6, β7 and the helix H1 (Figure 3a) and the changes are very similar to those observed when p53TAD2 (Figure 3b) and TFIIEαCTD (Supplementary Figure S3c) bind to Tfb1PH.

To confirm that $Rad2_{642–690}$ shares a common binding site on Tfb1PH with p53TAD2 and TFIIEαCTD (19), NMR competition experiments were performed. In the first experiment, we add a substoichiometric concentration of unlabeled Tfb1PH (0.4 mM) to a sample containing $^{15}$N-labeled p53TAD2 (0.5 mM) and, as expected, we observe significant changes in $^{1}$H and $^{15}$N chemical shifts in the $^{1}$H–$^{15}$N HSQC spectra of p53TAD2 (Figure 3c). We subsequently added an equimolar amount of unlabeled $Rad2_{642–690}$ (0.5 mM) to the $^{15}$N–p53TAD2–Tfb1PH sample and observe that the $^{1}$H and $^{15}$N resonances of p53TAD2 which shift upon formation of the p53TAD2–Tfb1PH complex returned to the values of the free form of p53TAD2 (Figure 3d). Taken together with previous results showing that TFIIEαCTD and p53TAD2 compete for binding to Tfb1PH (19), these results demonstrate that TFIIEαCTD, p53TAD2 and $Rad2_{642–690}$ all share for a common binding site on Tfb1PH.

### NMR structure determination of the $Rad2_{642–690}$–Tfb1PH complex

To structurally compare complexes of Tfb1PH involved in transcription and in DNA repair, we determined the structure of the $Rad2_{642–690}$–Tfb1PH complex. The structure of the $Rad2_{642–690}$–Tfb1PH complex (PDB code 2LOX) is well defined by the NMR data (Table 1). The 20 lowest-energy structures (Figure 4a) are characterized by good backbone geometry, no significant restraint violation and low pairwise rmsd values (Table 1). In complex with $Rad2_{642–690}$, the Tfb1PH structure is virtually identical to its free form showing a typical PH domain fold consisting of a seven-stranded β sandwich (β1–β7) flanked on one side by a long α helix (H1) (24). $Rad2_{642–690}$ exists in an extended conformation devoid of any regular secondary structural element with residues 664–678 forming the interface with Tfb1PH. This is consistent with the $^{1}$H–$^{15}$N HSQC spectra of the titration of $^{15}$N-labeled $Rad2_{642–690}$ with Tfb1PH as it is these residues that display significant changes in their $^{1}$H and $^{15}$N chemical shifts (Supplementary Figure S4).

### $Rad2_{642–690}$–Tfb1PH binding interface

In the complex, $Rad2_{642–690}$ binds in an extended form to two adjacent shallow grooves on the surface of Tfb1PH. The first groove is formed by residues Gln49, Ala50, Thr51, Pro52, Met59, Leu60, Arg61 and Met88 from

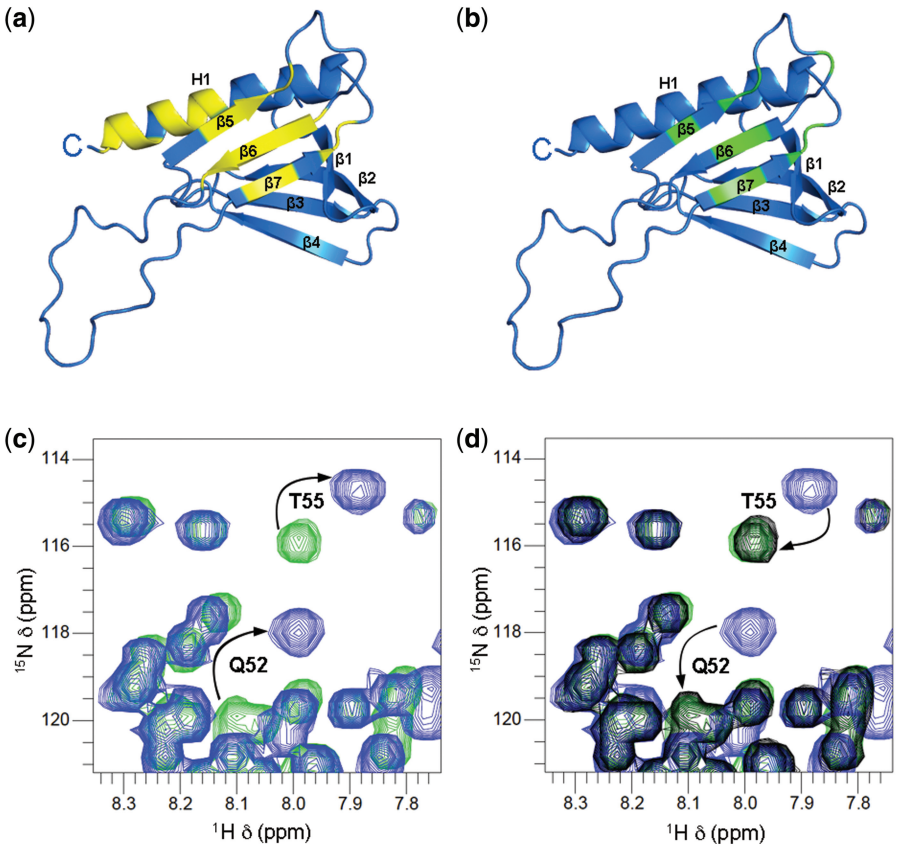


**Figure 3.** Rad2$_{642–690}$ and p53TAD2 share a common binding site on Tfb1PH. (**a** and **b**) Ribbon models of the 3D structure of Tfb1PH (blue; PDB code 1Y5O). The amino acids of $^{15}$N-labeled Tfb1PH showing a significant chemical shift change $\{\Delta\delta(\text{ppm}) > 0.15;\ \Delta\delta = [(0.17\Delta N_H)^2 + (\Delta H_N)^2]^{1/2}\}$ upon formation of a complex with either Rad2$_{642–690}$ (a) or p53TAD2 (b) are highlighted in yellow and green, respectively. (**c**) Overlay of a selected region from the $^1$H–$^{15}$N HSQC spectra of $^{15}$N-labeled p53TAD2 (0.5 mM) in the free form (green) and in the presence of unlabeled Tfb1PH (0.4 mM; blue). (**d**) Same overlay as in (c), but after the addition of unlabeled Rad2$_{642–690}$ (0.5 mM; black). Signals of p53TAD2 that undergo significant changes in $^1$H and $^{15}$N chemical shifts upon formation of the complex with Tfb1PH (c), and that return toward their original position following the addition of Rad2$_{642–690}$ (d) are indicated by arrows.

strands β5, β6 and β7 of Tfb1PH (Figure 4b). Phe670 of Rad2 inserts into this groove where it is in position to form a cation–π interaction with Arg61. In addition, Leu665 and Leu669 of Rad2 make van der Waals interactions with Met59 and Lys57 of Tfb1PH. The second groove is composed of Leu48, Ala50, Lys101 and Gln105, Ile108, Lys112 of Tfb1PH and accommodates Val673 and Thr675 of Rad2 (Figure 4c). Val673 is anchored on one side of this groove through van der Waals interactions of its two-methyl groups and the side chains of Leu48, Ala50, Lys101 and Gln105 of Tfb1PH. Thr675 is anchored on the other side of the groove where its methyl group interacts with the side chains of Gln105, Ile108 and Lys112.

Although the majority of the interactions within the two grooves are van der Waals contacts, an extensive series of positively charged residues on the surface of Tfb1PH (Lys47, Lys57, Arg61, Arg86, Lys97, Lys101 and Lys112) surround the two grooves, where they function to position the negatively charged Rad2$_{642–690}$. The NMR structures support the formation of two potential salt bridges between acidic residues of Rad2$_{642–690}$ and basic residues of Tfb1PH. The first one is between Glu667 of Rad2$_{642–690}$ and either Arg61 or Arg86 of Tfb1PH (Supplementary Figure S5a), and the second one is between Asp672 of Rad2$_{642–690}$ and Lys47 of Tfb1PH (Supplementary Figure S5b).

### A second acid-rich segment of the Rad2 spacer region binds to Tfb1PH

Previous studies have shown that several segments within the Rad2/XPG spacer region interact with numerous subunits of TFIIH (10–13). Therefore, the remaining residues of the Rad2 spacer region (residues 100–641) were analyzed for additional Tfb1PH-binding sites based on their sequence similarity to TFIIEαCTD, p53TAD2 or Rad2$_{642–690}$. Through this search, one potential site was identified between residues 359–383 (Rad2$_{359–383}$; Figure 5a), and ITC studies show that Rad2$_{359–383}$ binds to Tfb1PH ($K_d$ = 130 nM) with a similar affinity as Rad2$_{642–690}$ (Figure 5a). Interestingly, the predicted Tfb1PH-binding site within Rad2$_{359–383}$ is very similar to the Tfb1PH-binding site in Rad2$_{642–690}$.

To identify the mode of binding for Rad2$_{359–383}$ to Tfb1PH, NMR chemical shift perturbation and competition studies were performed. Addition of unlabeled

**Table 1.** NMR and refinement statistics for Rad2 in complex with Tfb1PH[a]

| | |
|---|---|
| NMR distance and dihedral constraints | |
| Distance constraints | |
| Total NOE | 1593 |
| Intra-residue | 377 |
| Inter-residue | |
| Sequential ($\|i-j\| = 1$) | 403 |
| Medium-range ($\|i-j\| < 4$) | 240 |
| Long-range ($\|i-j\| > 5$) | 480 |
| Intermolecular | 93 |
| Hydrogen bonds | 36 |
| Total dihedral angle restraints | 160 |
| $\phi$ | 80 |
| $\psi$ | 80 |
| Structure statistics | |
| Deviations from idealized geometry | |
| Distance constraints (Å) | 0.0197 ± 0.0004 |
| Dihedral angle constraints (°) | 0.237 ± 0.019 |
| Bond lengths (Å) | 0.00260 ± 0.00007 |
| Bond angles (°) | 0.423 ± 0.004 |
| Impropers (°) | 0.289 ± 0.008 |
| Ramachandran statistics (%)[b] | |
| Residues in most favored regions | 72.5 |
| Residues in additional allowed regions | 25.6 |
| Residues in generously allowed regions | 1.5 |
| Residues in disallowed regions | 0.4 |
| Average pairwise rmsd (Å)[c] | |
| Heavy | 1.09 ± 0.10 |
| Backbone | 0.42 ± 0.08 |

[a]The 20 conformers with the lowest energies were selected for statistical analysis.
[b]Based on PROCHECK-NMR analysis.
[c]Only residues 5–63 and 86–112 of Tfb1PH and residues 669–675 of Rad2 were used for the rmsd calculations. Residues at the N terminus (1–4), at the C terminus (113–115), and in the flexible loop (64–85) of Tfb1PH, as well as residues at the N terminus (642–668) and at the C terminus (676–690) of Rad2 were not included in the calculation.

$Rad2_{359–383}$ to $^{15}$N-labeled Tfb1PH causes significant changes in the $^{1}$H and $^{15}$N chemical shifts for several Tfb1PH signals in the $^{1}$H–$^{15}$N HSQC spectra (Supplementary Figure S6). When mapped onto the structure of Tfb1PH, the residues exhibiting significant chemical shift changes are located in strands β5, β6, β7 and the helix H1 (Figure 5b) and the changes are very similar to those observed with $Rad2_{642–690}$ (Figure 3a). NMR competition experiments further demonstrate that $Rad2_{359–383}$ and $Rad2_{642–690}$ compete for binding to Tfb1PH (Figure 5c and d).

### TFIIH binding sites of Rad2 enhance resistance to UV irradiation

To examine the *in vivo* role of the two Tfb1PH-binding sites of Rad2 following exposure to UV irradiation, yeast mutants were created in which the key segments were deleted either alone or in combination. Initially, either residues 367–378 (*rad2-ΔD2*) or residues 642–760 (*rad2-ΔD3*) of *RAD2* were deleted and the resulting mutant strains were tested for survival under increasing doses of UV irradiation. In comparison to the wild-type *RAD2* strain, neither of the two mutant strains shows an enhancement in sensitivity to UV radiation (Figure 6a). Given that both single deletions fail to induce a UV-sensitive phenotype, a third mutant was constructed in which both residues 367–378 and residues 642–760 of Rad2 (*rad2-ΔD2D3*) were deleted. When compared to the *RAD2* strain, survival curves again indicate that the *rad2-ΔD2D3* fails to induce an enhancement in sensitivity to UV irradiation (Figure 6a).

Previous studies have shown that residues 225–231 within the spacer region of XPG (XPGΔ225–231) play an important role in binding to TFIIH, and these residues are deleted in certain patients with XP/CS syndrome (11). To determine if the corresponding residues of Rad2 (residues 228–237) play an important role in yeast survival following exposure to UV irradiation, a mutant in which residues 228–237 of Rad2 were deleted (*rad2-ΔD1*) was tested for its survival following exposure to UV irradiation. Consistent with what has been observed with XPGΔ225–231 patients, the *rad2-ΔD1* yeast display a significant enhancement in sensitivity to UV irradiation in comparison to the *RAD2* strain (Figure 6b). However, the *rad2-ΔD1* strain is significantly less sensitive to UV irradiation than *rad2* (Figure 6b).

Since multiple segments of the Rad2 spacer region participate in binding to TFIIH, we next tested if mutations of key residues within the Tfb1PH-binding sites of Rad2 could enhance the photosensitivity of the *rad2-ΔD1* strain. To do this, a yeast strain deleted of residues 228–237 in combination with proline mutations of the four key hydrophobic residues (W372P, V375P, F670P and V673P) within the Tfb1PH-binding sites of Rad2 (*rad2-ΔD1PPPP*) was prepared and tested for survival following exposure to UV irradiation. Interestingly, the *rad2-ΔD1PPPP* yeast display a significant enhancement in sensitivity to UV irradiation in comparison to *rad2-ΔD1* (Figure 6b). These results are consistent with the hypothesis that multiple segments of the Rad2 spacer region participate in a series of interactions with TFIIH and it is not the result of decreased levels of Rad2 as the Rad2 mutant proteins are expressed at similar levels as the wild-type Rad2 (Supplementary Figure S1b).

## DISCUSSION

TFIIH is unique among the GTFs in that it also plays an important role in DNA repair as a key component of the NER pathway. In NER, TFIIH serves several functions through the helicase activity of its XPD/Rad3 and XPB/Ssl2 subunits as well as through protein–protein interactions with other repair factors. It has been previously shown that multiple subunits of TFIIH interact with several other DNA repair factors including XPC/Rad4, XPG/Rad2 and CSB/Rad26, and these interactions help to stabilize the repair complex (13,43). Despite the importance of these protein–protein interactions, prior to this work there were no high-resolution structures reported of a complex involving any of the subunits of TFIIH and a repair factor. In this manuscript, we have functionally and structurally examined the interaction between the Tfb1 subunit of TFIIH and the repair factor Rad2 from budding yeast. We demonstrate that deletion of either the

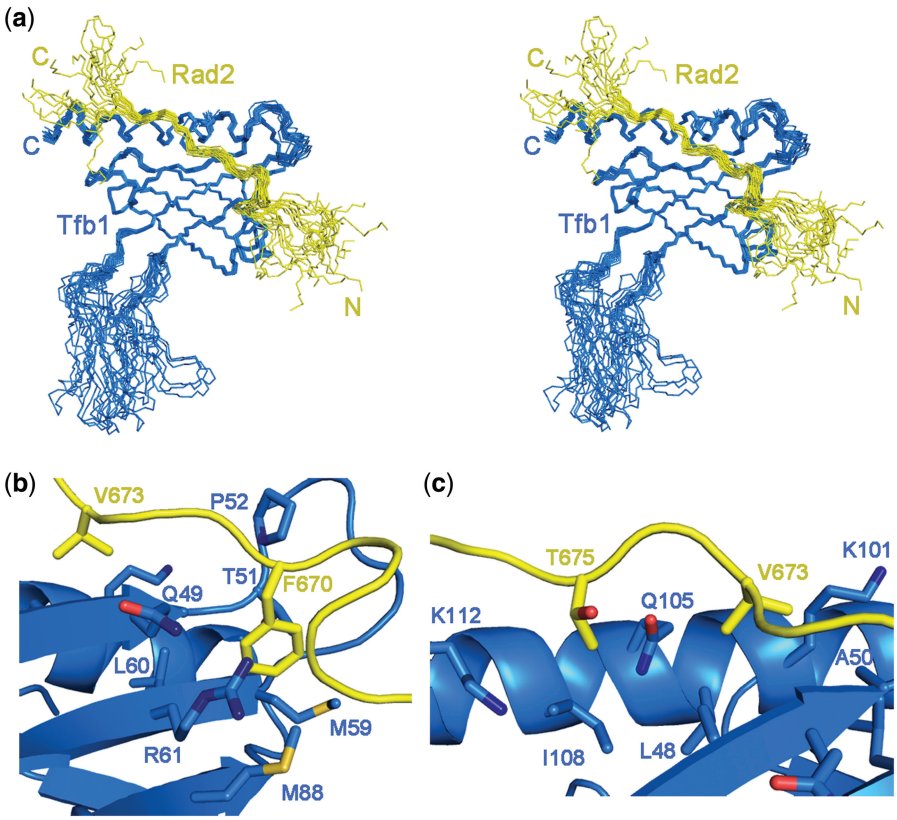


**Figure 4.** NMR structure of the $Rad2_{642–690}$–Tfb1PH complex. (**a**) Stereo view of the 20 lowest-energy structures of the complex between Tfb1PH (blue) and $Rad2_{642–690}$ (yellow; PDB code 2LOX). The structures were superimposed using the backbone atoms C′, $C^{\alpha}$ and N of residues 4–65 and 85–112 of Tfb1PH and residues 661–680 of $Rad2_{642–690}$. (**b**) Ribbon representation of Tfb1PH (blue) and backbone trace of the region of $Rad2_{642–690}$ (yellow) interacting in the first groove. In this groove, Phe670 of Rad2 forms a cation–π interaction with Arg61 of Tfb1 and van der Waals interaction with Met59 and Lys57. (**c**) Ribbon representation of Tfb1PH (blue) and backbone trace of the region of $Rad2_{642–690}$ (yellow) interacting in the second groove. On one side of the groove Val673 of Rad2 is inserted where it interacts with Leu48, Ala50, Lys101 and Gln105 of Tfb1. On the other side of the groove, Thr675 of Rad2 interacts with Gln105, Ile108 and Lys112 of Tfb1.

Tfb1PH or several different segments of the spacer region of Rad2 yield yeast mutants that display an enhanced sensitivity to UV irradiation. By ITC analysis, we show that two acid-rich segments of the Rad2 spacer region bind to Tfb1PH with high affinity. NMR chemical shift perturbation and competition studies indicate that the two segments of Rad2 ($Rad2_{359–383}$ and $Rad2_{642–690}$) compete for a common binding site on Tfb1PH and that this is the same site required for interaction with TFIIEαCTD and p53TAD2. The 3D structure of a complex formed by Tfb1PH and one of the acid-rich segments of Rad2 ($Rad2_{642–690}$) reveals that Rad2 binds to Tfb1PH in an extended form much like TFIIEαCTD, but not in a helical structure as observed with p53TAD2 and VP16C (20–22).

Rad2 and XPG are unique members of the FEN-1 nuclease family by virtue of the fact that they directly interact with TFIIH and contain an extended spacer region (>600 amino acids) between their highly conserved N and I regions. A direct comparison of the spacer region of Rad2 and XPG is difficult since their sequences are not as highly conserved as their N and I regions, and this is consistent with the fact that both spacer regions are predicted to be intrinsically unstructured. However, the XPG and Rad2 spacer regions do share common features including a high percentage of acidic amino acids and the ability to interact with multiple subunits of TFIIH including p62/Tfb1. Based on binding studies, it has been proposed that TFIIH recruits XPG/Rad2 to the repair complex through a series of weak interactions and that the spacer region plays a key role in this recruitment (10). Our results demonstrating that two segments within the spacer region of Rad2 bind the Tfb1PH are consistent with the idea of multiple interactions between Rad2 and TFIIH. Although deletion of either or both of the Tfb1PH binding sites does not directly result in a UV phenotype in yeast, mutations of the key hydrophobic residues within these binding sites enhances the sensitivity when combined with deletion of residues 228–237 that are homologous to residues 225–231 of XPG. This region of XPG has been shown to be important for binding to TFIIH and it is deleted in patients with XP/CS (Xeroderma Pigmentosum/Cockayne Syndrome) (11). It is also clear that this domain is important for repair of UV-induced DNA damage in yeast, but the exact mechanism by which this region interacts with TFIIH is currently unknown. However, our *in vivo* results with the mutations within these three segments of Rad2 in yeast are consistent with

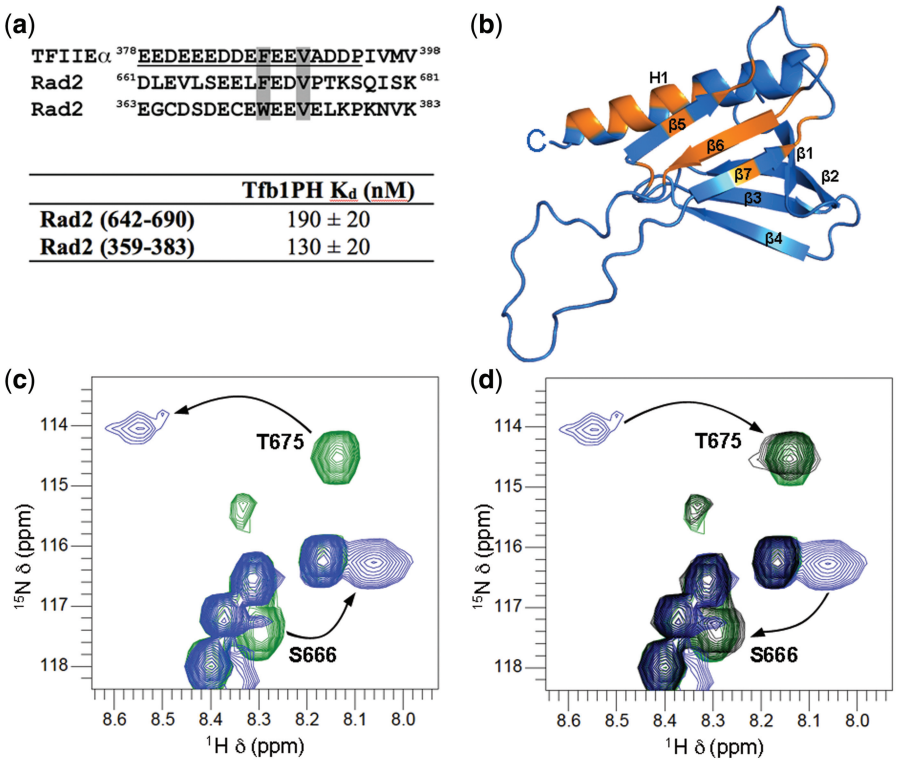


**Figure 5.** The Rad2 spacer region contains a second high-affinity Tfb1PH-binding site. (**a**) (*Top*) Identification of amino acid segments located between residues 363–382 from the Rad2 spacer region that align with the Tfb1PH-binding sites from TFIIEαCTD and $Rad2_{642–690}$. In the alignments, the residues of TFIIEαCTD and $Rad2_{642–690}$ that form the binding interface with p62PH/Tfb1PH are underlined and crucial hydrophobic residues are shaded in gray. (*Bottom*) Dissociation constant ($K_d$) values for the binding of $Rad2_{359–383}$ and $Rad2_{642–690}$ with Tfb1PH as determined by ITC analysis. (**b**) Ribbon models of the 3D structure of Tfb1PH (blue; PDB code 1Y5O). The amino acids of $^{15}$N-labeled Tfb1PH showing a significant chemical shift change $\{\Delta\delta(\text{ppm}) > 0.15;\ \Delta\delta = [(0.17\Delta N_H)^2 + (\Delta H_N)^2]^{1/2}\}$ upon formation of a complex with $Rad2_{359–383}$ are highlighted in orange. (**c**) Overlay of a selected region from the $^1$H–$^{15}$N HSQC spectra of $^{15}$N-labeled $Rad2_{642–690}$ (0.5 mM) in the free form (green) and in the presence of unlabeled Tfb1PH (0.4 mM; blue). (**d**) Same overlay as in c, but after the addition of unlabeled $Rad2_{359–383}$ (1.0 mM; black). Signals of $Rad2_{642–690}$ that undergo significant chemical shift changes in $^1$H and $^{15}$N chemical shifts upon formation of the complex with Tfb1PH (c), and that return toward their original position following the addition of $Rad2_{359–383}$ (d) are indicated by arrows.

the critical role of residues 225–231 in DNA repair in humans and the hypothesis that the Rad2 spacer forms multiple interactions with TFIIH that are required for NER.

It is interesting to compare our structure of the $Rad2_{642–690}$–Tfb1PH complex with the other structures of complexes involving Tfb1PH and p62PH. Structures have been solved with Tfb1PH bound to three acidic TADs [p53TAD2 (20), VP16C (21) and EKLFTAD2 (44)] and p62PH bound to TFIIEαCTD (22). p53TAD2 and VP16C both form 9-residue α-helices upon binding to Tfb1PH in a coupled folding and binding mechanism. Comparison of the p53TAD2–Tfb1PH structure with the $Rad2_{642–690}$–Tfb1PH structure indicates that p53TAD2 and $Rad2_{642–690}$ bind along slightly different grooves on Tfb1PH, but share a common anchor point involving Phe54 on p53TAD2 and Phe670 on Rad2 (Figure 7a and b–e). In contrast, EKLFTAD2 and TFIIEαCTD bind in more elongated conformation as seen with $Rad2_{642–690}$ and follow very similar trajectories. In particular, there are a number of similarities between the interface of the $Rad2_{642–690}$–Tfb1PH complex and the interface of the TFIIEαCTD–p62PH complex (Figure 7a–f). The N-terminal region of TFIIEαCTD binds to p62PH in an extended form and interacts with strands β5, β6 and β7. $Rad2_{642–690}$ binds to Tfb1PH in a very similar extended conformation and the interface it forms with Tfb1PH is almost identical (Figure 7a–c). In particular, Phe670 and Val673 of Rad2 make similar van der Waals contacts as Phe387 and Val390 of TFIIEαCTD in the TFIIEαCTD–p62PH complex (Figure 7d–f). In addition, there are similar electrostatic interactions in both complexes between positively charged residues of the PH domains and negatively charged residues of either Rad2 or TFIIEα. The main difference between the two structures is that TFIIEαCTD contains an ordered region that separates two disordered acidic regions (Figure 7c). NMR studies with a longer segment of the Rad2 spacer region ($Rad2_{642–760}$) indicate that this segment does not contain a folded domain in the free form (Supplementary Figure S2), as observed with the free form of TFIIEαCTD.

Like PH domains in many cytosolic signaling proteins, the Tfb1PH/p62PH provides an excellent scaffold for protein–protein interactions that are important for the regulation of both transcription and NER in the

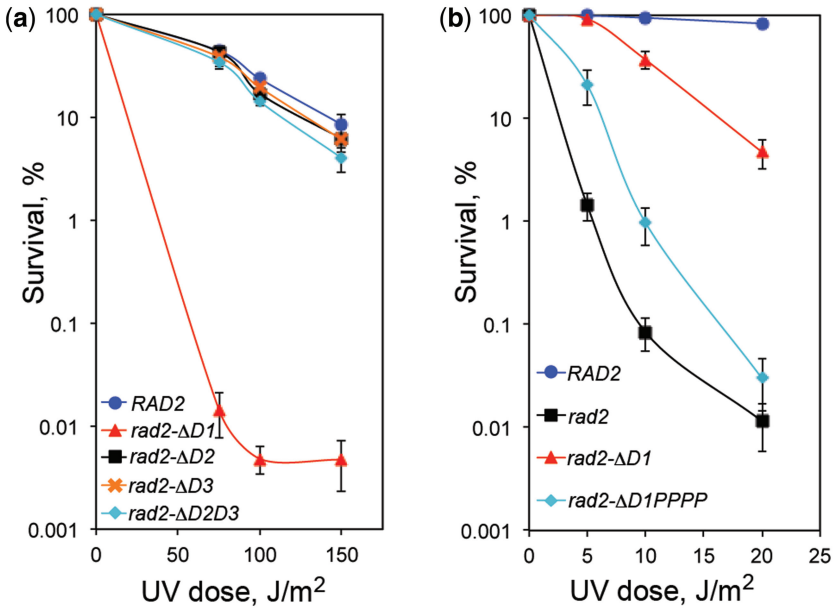


**Figure 6.** Multiple regions of the Rad2 spacer are required for repair of UV damage. (**a**) The survival of *RAD2* (blue), *rad2-ΔD1* (red), *rad2-ΔD2* (black), *rad2-ΔD3* (orange) and *rad2-ΔD2D3* (aqua) yeast was determined following increasing doses of UV irradiation. The *y*-axis represents the percentage of surviving cells (normalized to the number of viable cells not exposed to UV light) and the *x*-axis shows the energy level of the UV irradiation applied (J/m$^2$). The results are the mean ± SEM of three independent experiments. (**b**) The survival of *RAD2* (blue), *rad2* (black), *rad2-ΔD1* (red) and *rad2-ΔD1PPPP* (aqua) yeast was determined following increasing doses of UV irradiation. The *y*-axis represents the percentage of surviving cells (normalized to the number of viable cells not exposed to UV light) and the *x*-axis shows the energy level of the UV irradiation applied (J/m$^2$). The results are the mean ± SEM of four independent experiments.

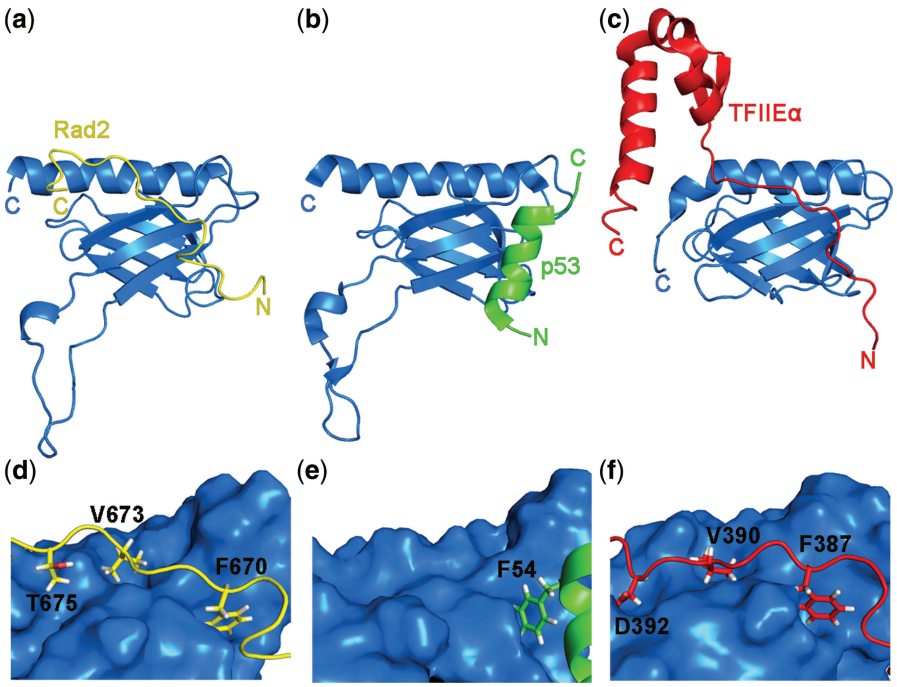


**Figure 7.** The structures of the Rad2$_{642–690}$–Tfb1PH and TFIIEαCTD–p62PH interfaces are remarkably similar. (**a–c**) Ribbon diagrams of the lowest energy structures of the Rad2$_{642–690}$–Tfb1PH (a; PDB code 2LOX), the p53TAD2–Tfb1PH (b; PDB code 2GS0) and the TFIIEαCTD–p62PH (c; PDB code 2RNR) complexes. Tfb1PH (a and b) and p62PH (c) are shown in blue, Rad2$_{642–690}$ (a) in yellow, p53TAD2 (b) in green and TFIIEαCTD (c) in red. In panels (**d–f**), the 3D structure of Tfb1PH (d–e) and p62PH (f) are shown as molecular surfaces (blue) and Rad2$_{642–690}$ (d), p53TAD2 (e) and TFIIEαCTD (f) are shown as ribbons in yellow, green and red, respectively. Selected residues of Rad2$_{642–690}$ (d), p53TAD2 (e) and TFIIEαCTD (f) at the binding interface are also shown.

nucleus. The similarity between the $Rad2_{642–690}$–Tfb1PH and the TFIIEαCTD–p62PH interfaces allows us to define a Tfb1PH-binding motif that consists of an aromatic residue (W or F) followed by two acidic residues and a valine residue located within a highly acidic segment (see Figures 2a and 5a). The reason for the two Tfb1PH binding motifs within the spacer region of Rad2 is not clear at this point in time, but this may reflect the highly dynamic nature of the TFIIH–Rad2 complex during NER. In addition, the remarkable similarity between the interfaces of the $Rad2_{642–690}$–Tfb1PH and the TFIIEαCTD–p62PH complexes provides a clear mechanistic link for the role of the Tfb1/p62 subunit of TFIIH in both transcription and NER.

## ACCESSION NUMBER

2LOX.

## SUPPLEMENTARY DATA

Supplementary Data are available at NAR Online: Supplementary Tables 1 and 2, Supplementary Figures 1–6, Supplementary Methods and Supplementary Reference [45].

## ACKNOWLEDGEMENTS

We would like to thank Dr Steve Hahn and Dr Pascal Chartrand for strains and clones, Dr Lawrence Myers for the anti-Tfb1 antibody, Aurélie Bernier for help with protein purification and Dr Tara Sprules for assistance with several NMR experiments.

## FUNDING

Canadian Cancer Society (to J.G.O.). J.L.-V. is a Vanier Canada Graduate Scholar from the Canadian Institutes of Health Research. L.C. is a postdoctoral fellow of the Natural Sciences and Engineering Research Council of Canada CREATE program. P.L. is a Canadian Research Chair in Structural Biology and Engineering of RNA. NMR experiments of 800MHz were recorded at the Québec/Eastern Canada High Field NMR Facility, supported by the Natural Sciences and Engineering Research Council of Canada. Funding for open access charge: Canadian Cancer Society (grant #019369).

*Conflict of interest statement*. None declared.

## REFERENCES

1. Le May,N., Egly,J.M. and Coin,F. (2010) True lies: the double life of the nucleotide excision repair factors in transcription and DNA repair. *J. Nucleic Acids*, **2010**, Article ID 616342.
2. Tirode,F., Busso,D., Coin,F. and Egly,J.M. (1999) Reconstitution of the transcription factor TFIIH: assignment of functions for the three enzymatic subunits, XPB, XPD and cdk7. *Mol. Cell*, **3**, 87–95.
3. Lu,H., Zawel,L., Fisher,L., Egly,J.M. and Reinberg,D. (1992) Human general transcription factor IIH phosphorylates the C-terminal domain of RNA polymerase II. *Nature*, **358**, 641–645.
4. Araujo,S.J., Nigg,E.A. and Wood,R.D. (2001) Strong functional interactions of TFIIH with XPC and XPG in human DNA nucleotide excision repair, without a preassembled repairosome. *Mol. Cell. Biol.*, **21**, 2281–2291.
5. Sung,P., Guzder,S.N., Prakash,L. and Prakash,S. (1996) Reconstitution of TFIIH and requirement of its DNA helicase subunits, Rad3 and Rad25, in the incision step of nucleotide excision repair. *J. Biol. Chem.*, **271**, 10821–10826.
6. Friedberg,E.C., Walker,G.C., Siede,W., Wood,R.D., Schultz,T. and Ellenberger,T. (2005) *DNA Repair and Mutagenesis*. ASM Press, Washington, DC.
7. Schärer,O.D. (2008) The molecular basis for different disease states caused by mutations in TFIIH and XPG. *DNA Repair*, **7**, 339–344.
8. Lieber,M.R. (1997) The FEN-1 family of structure-specific nucleases in eukaryotic DNA replication, recombination and repair. *Bioessays*, **19**, 233–240.
9. Tsutakawa,S.E., Classen,S., Chapados,B.R., Arvai,A.S., Finger,L.D., Guenther,G., Tomlinson,C.G., Thompson,P., Sarker,A.H., Shen,B. *et al*. (2011) Human flap endonuclease structures, DNA double-base flipping, and a unified understanding of the FEN1 superfamily. *Cell*, **145**, 198–211.
10. Dunand-Sauthier,I., Hohl,M., Thorel,F., Jaquier-Gubler,P., Clarkson,S.G. and Scharer,O.D. (2005) The spacer region of XPG mediates recruitment to nucleotide excision repair complexes and determines substrate specificity. *J. Biol. Chem.*, **280**, 7030–7037.
11. Thorel,F., Constantinou,A., Dunand-Sauthier,I., Nouspikel,T., Lalle,P., Raams,A., Jaspers,N.G., Vermeulen,W., Shivji,M.K., Wood,R.D. *et al*. (2004) Definition of a short region of XPG necessary for TFIIH interaction and stable recruitment to sites of UV damage. *Mol. Cell. Biol.*, **24**, 10670–10680.
12. Iyer,N., Reagan,M.S., Wu,K.J., Canagarajah,B. and Friedberg,E.C. (1996) Interactions involving the human RNA polymerase II transcription/nucleotide excision repair complex TFIIH, the nucleotide excision repair protein XPG, and Cockayne syndrome group B (CSB) protein. *Biochemistry*, **35**, 2157–2167.
13. Bardwell,A.J., Bardwell,L., Iyer,N., Svejstrup,J.Q., Feaver,W.J., Kornberg,R.D. and Friedberg,E.C. (1994) Yeast nucleotide excision repair proteins Rad2 and Rad4 interact with RNA polymerase II basal transcription factor b (TFIIH). *Mol. Cell. Biol.*, **14**, 3569–3576.
14. Zotter,A., Luijsterburg,M.S., Warmerdam,D.O., Ibrahim,S., Nigg,A., van Cappellen,W.A., Hoeijmakers,J.H.J., van Driel,R., Vermeulen,W. and Houtsmuller,A.B. (2006) Recruitment of the nucleotide excision repair endonuclease XPG to sites of UV-induced DNA damage depends on functional TFIIH. *Mol. Cell. Biol.*, **26**, 8868–8879.
15. Lehmann,A.R. (2003) DNA repair-deficient diseases, xeroderma pigmentosum, Cockayne syndrome and trichothiodystrophy. *Biochimie*, **85**, 1101–1111.
16. Hohl,M., Dunand-Sauthier,I., Staresincic,L., Jaquier-Gubler,P., Thorel,F., Modesti,M., Clarkson,S.G. and Scharer,O.D. (2007) Domain swapping between FEN-1 and XPG defines regions in XPG that mediate nucleotide excision repair activity and substrate specificity. *Nucleic Acids Res.*, **35**, 3053–3063.
17. Matsui,P., DePaulo,J. and Buratowski,S. (1995) An interaction between the Tfb1 and Ssl1 subunits of yeast TFIIH correlates with DNA repair activity. *Nucleic Acids Res.*, **23**, 767–772.
18. Gervais,V., Lamour,V., Jawhari,A., Frindel,F., Wasielewski,E., Dubaele,S., Egly,J.M., Thierry,J.C., Kieffer,B. and Poterszman,A. (2004) TFIIH contains a PH domain involved in DNA nucleotide excision repair. *Nat. Struct. Mol. Biol.*, **11**, 616–622.
19. Di Lello,P., Miller Jenkins,L.M., Mas,C., Langlois,C., Malitskaya,E., Fradet-Turcotte,A., Archambault,J., Legault,P. and Omichinski,J.G. (2008) p53 and TFIIEalpha share a common binding site on the Tfb1/p62 subunit of TFIIH. *Proc. Natl Acad. Sci. USA*, **105**, 106–111.
20. Di Lello,P., Jenkins,L.M., Jones,T.N., Nguyen,B.D., Hara,T., Yamaguchi,H., Dikeakos,J.D., Appella,E., Legault,P. and Omichinski,J.G. (2006) Structure of the Tfb1/p53 complex: insights into the interaction between the p62/Tfb1 subunit of TFIIH and the activation domain of p53. *Mol. Cell*, **22**, 731–740.

21. Langlois,C., Mas,C., Di Lello,P., Jenkins,L.M., Legault,P. and Omichinski,J.G. (2008) NMR structure of the complex between the Tfb1 subunit of TFIIH and the activation domain of VP16: structural similarities between VP16 and p53. *J. Am. Chem. Soc.*, **130**, 10596–10604.
22. Okuda,M., Tanaka,A., Satoh,M., Mizuta,S., Takazawa,M., Ohkuma,Y. and Nishimura,Y. (2008) Structural insight into the TFIIE-TFIIH interaction: TFIIE and p53 share the binding region on TFIIH. *EMBO J.*, **27**, 1161–1171.
23. Kaiser,C., Michaelis,S. and Mitchell,A. (1994) *Methods in Yeast Genetics*. Cold Spring Harbor Laborator Press, Cold Spring Harbor, NY.
24. Di Lello,P., Nguyen,B.D., Jones,T.N., Potempa,K., Kobor,M.S., Legault,P. and Omichinski,J.G. (2005) NMR structure of the amino-terminal domain from the Tfb1 subunit of TFIIH and characterization of its phosphoinositide and VP16 binding sites. *Biochemistry*, **44**, 7678–7686.
25. Houtman,J.C., Higashimoto,Y., Dimasi,N., Cho,S., Yamaguchi,H., Bowden,B., Regan,C., Malchiodi,E.L., Mariuzza,R., Schuck,P. *et al.* (2004) Binding specificity of multiprotein signaling complexes is determined by both cooperative interactions and affinity preferences. *Biochemistry*, **43**, 4170–4178.
26. Nguyen,B.D., Di Lello,P., Legault,P. and Omichinski,J.G. (2005) 1H, 15N, and 13C resonance assignment of the amino-terminal domain of the Tfb1 subunit of yeast TFIIH. *J. Biomol. NMR*, **31**, 173–174.
27. Kay,L.E., Xu,G.Y. and Yamazaki,T. (1994) Enhanced-sensitivity triple-resonance spectroscopy with minimal H2O saturation. *J. Magn. Reson. A*, **109**, 129–133.
28. Wittekind,M. and Mueller,L. (1993) HNCACB, a high-sensitivity 3D NMR experiment to correlate amide-proton and nitrogen resonances with the alpha- and beta-carbon resonances in proteins. *J. Magn. Reson. B*, **101**, 201–205.
29. Grzesiek,S. and Bax,A. (1992) Correlating backbone amide and side chain resonances in larger proteins by multiple relayed triple resonance NMR. *J. Am. Chem. Soc.*, **114**, 6291–6293.
30. Logan,T.M., Olejniczak,E.T., Xu,R.X. and Fesik,S.W. (1992) Side chain and backbone assignments in isotopically labeled proteins from two heteronuclear triple resonance experiments. *FEBS Lett.*, **314**, 413–418.
31. Ikura,M., Kay,L.E. and Bax,A. (1991) Improved three-dimensional 1H-13C-1H correlation spectroscopy of a 13C-labeled protein using constant-time evolution. *J. Biomol. NMR*, **1**, 299–304.
32. Yamazaki,T., Forman-Kay,J.D. and Kay,L.E. (1993) Two-dimensional NMR experiments for correlating carbon-13 beta and proton delta/epsilon chemical shifts of aromatic residues in 13C-labeled proteins via scalar couplings. *J. Am. Chem. Soc.*, **115**, 11054–11055.
33. Zhang,O., Kay,L.E., Olivier,J.P. and Forman-Kay,J.D. (1994) Backbone 1H and 15N resonance assignments of the N-terminal SH3 domain of drk in folded and unfolded states using enhanced-sensitivity pulsed field gradient NMR techniques. *J. Biomol. NMR*, **4**, 845–858.
34. Pascal,S.M., Muhandiram,D.R., Yamazaki,T., Forman-Kay,J.D. and Kay,L.E. (1994) Simultaneous acquisition of $^{15}$N- and $^{13}$C-edited NOE spectra of proteins dissolved in $H_2O$. *J. Magn. Reson.*, **103**, 197–201.
35. Delaglio,F., Grzesiek,S., Vuister,G.W., Zhu,G., Pfeifer,J. and Bax,A. (1995) NMRPipe: a multidimensional spectral processing system based on UNIX pipes. *J. Biomol. NMR*, **6**, 277–293.
36. Johnson,B.A. (2004) Using NMRView to visualize and analyze the NMR spectra of macromolecules. *Methods Mol. Biol.*, **278**, 313–352.
37. Vranken,W.F., Boucher,W., Stevens,T.J., Fogh,R.H., Pajon,A., Llinas,M., Ulrich,E.L., Markley,J.L., Ionides,J. and Laue,E.D. (2005) The CCPN data model for NMR spectroscopy: development of a software pipeline. *Proteins*, **59**, 687–696.
38. Shen,Y., Delaglio,F., Cornilescu,G. and Bax,A. (2009) TALOS+: a hybrid method for predicting protein backbone torsion angles from NMR chemical shifts. *J. Biomol. NMR*, **44**, 213–223.
39. Brunger,A.T., Adams,P.D., Clore,G.M., DeLano,W.L., Gros,P., Grosse-Kunstleve,R.W., Jiang,J.S., Kuszewski,J., Nilges,M., Pannu,N.S. *et al.* (1998) Crystallography & NMR system: a new software suite for macromolecular structure determination. *Acta Crystallogr. D Biol. Crystallogr.*, **54**, 905–921.
40. Laskowski,R.A., Rullmannn,J.A., MacArthur,M.W., Kaptein,R. and Thornton,J.M. (1996) AQUA and PROCHECK-NMR: programs for checking the quality of protein structures solved by NMR. *J. Biomol. NMR*, **8**, 477–486.
41. Koradi,R., Billeter,M. and Wuthrich,K. (1996) MOLMOL: a program for display and analysis of macromolecular structures. *J. Mol. Graph.*, **14**, 51–55.
42. The PyMOL Molecular Graphics System, Version 1.2r3pre, Schrödinger, LLC.
43. Tantin,D. (1998) RNA polymerase II elongation complexes containing the Cockayne syndrome group B protein interact with a molecular complex containing the transcription factor IIH components xeroderma pigmentosum B and p62. *J. Biol. Chem.*, **273**, 27794–27799.
44. Mas,C., Lussier-Price,M., Soni,S., Morse,T., Arseneault,G., Di Lello,P., Lafrance-Vanasse,J., Bieker,J.J. and Omichinski,J.G. (2011) Structural and functional characterization of an atypical activation domain in erythroid Kruppel-like factor (EKLF). *Proc. Natl Acad. Sci. USA*, **108**, 10484–10489.
45. Elagoz,A., Callejo,M., Armstrong,J. and Rokeach,L.A. (1999) Although calnexin is essential in *S. pombe*, its highly conserved central domain is dispensable for viability. *J. Cell Sci.*, **112**, 4449–4460.